Phase-Tailored OTFS Waveform with Reduced Sidelobes for ISAC Systems

Nazila Karimian-Sichani[1], Saeid Sedighi[2], Mohammad Alaee-Kerahroodi[3], Maria S. Greco[1], Fulvio Gini[1], Bhavani Shankar M. R.[3]

[1]*Department of Information Engineering, University of Pisa, Pisa, Italy.*
[2] *Valeo Switches and Sensors GmbH.*
[3]*Interdisciplinary Centre for Security, Reliability and Trust (SnT), University of Luxembourg, Luxembourg.*

***Abstract*—Integrated Sensing and Communication (ISAC) systems combine radar sensing and communication to improve spectral and hardware efficiency in 6G networks. The emerging Orthogonal Time Frequency Space (OTFS) modulation is well-suited for ISAC due to its robustness in the Delay-Doppler (DD) domain compared to traditional Orthogonal Frequency Division Multiplexing (OFDM). Despite its advantages, OTFS exhibits high sidelobe levels that affect sensing performance. To further enhance the radar sensing aspect of an OTFS-based ISAC system, we design a phase matrix to optimize the OTFS waveform. Our goal is to reduce the sidelobe levels of the 2D Ambiguity Function (AF) for the phase-tailored OTFS waveform. Specifically, we formulate an optimization problem to minimize the AF Peak Sidelobe Level (PSL) by introducing an additional degree of freedom for each communication symbol, thereby improving sensing performance while preserving similar communication efficiency. We solve the related non-convex NP-hard optimization problem and propose an Alternative Optimization (AO)-based algorithm. By decomposing the problem into two subproblems, one convex and the other is solved using Projected Gradient Descent (PGD), we iteratively update the variables until convergence. This approach effectively minimizes the PSL, improving target resolution and reducing interference. Simulation results show that the proposed method efficiently reduces the sidelobe levels and improves the AF, leading to increased sensing performance.**

***Index Terms*—OTFS, OFDM, Automotive Radar, Ambiguity Function, PMCW, FMCW.**

I. Introduction

Sixth-generation (6G) wireless communication builds on the advancements of 5G but introduces new technologies such as Integrated Sensing And Communication (ISAC), enabling real-time environmental awareness by merging radar and communication functions into a unified framework [1]–[3]. This integration is crucial for applications like autonomous driving, smart cities, and advanced vehicular networks, where efficient spectrum utilization and high-resolution sensing are essential.

A key enabler of ISAC is waveform design for Joint Radar and Communication (JRC), where emerging Orthogonal Time Frequency Space (OTFS) modulation, [4], [5], has gained attention for its superior performance in dynamic environments. Unlike conventional Orthogonal Frequency Division Multiplexing (OFDM), which operates in the Time-Frequency (TF) domain, OTFS maps data onto the Delay-Doppler (DD) domain, making it more resilient to high-mobility challenges such as Doppler shifts and multipath fading [6]. This property enhances radar sensing by enabling accurate target range and velocity estimation, crucial for real-time tracking in vehicular networks and smart infrastructure. Additionally, OTFS-based radar systems offer improved spectral efficiency, reduced Peak-to-average Power Ratio (PAPR), and greater resilience to channel variations compared to OFDM, positioning it as a strong candidate for next-generation ISAC applications in high-speed wireless environments.

While OTFS has been studied for its effectiveness in communication systems [4], [7]–[11], it has also been explored for radar sensing, contributing to target detection and parameter estimation [12]–[19]. Its inherent DD representation aligns with radar signal processing techniques, allowing for range and velocity estimation comparable to or, in some cases, better than OFDM. Although OTFS does not directly replicate classical radar waveforms such as Frequency Modulated Continuous Wave (FMCW) and Phase Modulated Continuous Wave (PMCW), it offers a flexible alternative for radar applications in ISAC systems. Studies show that OTFS-based radar can detect and track multiple targets in dense environments, making it a viable option for automotive and defense applications.

On the other hand, we showed in [20] that OTFS has high sidelobe levels, potentially masking weak targets or causing interference. To address this, we designed a phase matrix using the Coordinate Descent (CD) framework to minimize the Integrated Side-lobe Level (ISL) of the Ambiguity Function (AF) range cut, the focus was primarily on reducing sidelobes in the range dimension using discrete phase values. However, for improved radar performance, it is essential to minimize sidelobes in both the range and Doppler dimensions.

The AF plays a key role in balancing range and Doppler resolution in sensing applications. The Peak Side-lobe Level (PSL) of the AF directly impacts radar resolution, with lower sidelobes reducing interference and enhancing reliability [21]. In this paper, we extend our previous work by designing a phase matrix to reduce 2D AF sidelobes across both range

*The work of Nazila Karimian, M.Sabrina Greco and Fulvio Gini was supported by the European Union under the Italian National Recovery and Resilience Plan (PNRR) of NextGenerationEU partnership on "Telecommunications of the Future" (PE00000001 - program "RESTART"), CUP E63C22002040007 - D.D. n.1549 of 11/10/2022. The work of Mohammad Alaee-Kerharoodi and Bhavani Shankar M. R. was supported by FNR CORE INTER project SENCOM: C20/IS/14799710/SENCOM.

and Doppler dimensions. We formulate an optimization problem with continuous phase constraint (unimodular waveform), allowing greater control over the entire AF plane, and propose a solution to the associated non-convex problem.

The rest of this paper is organized as follows. Section II introduces OTFS modulation and its AF. Section III presents the problem formulation and solution for designing the phase matrix to minimize the AF PSL of the OTFS waveform. Numerical results for the proposed algorithm are provided in Section IV, and conclusions are drawn in Section V [1].

II. OTFS SIGNAL MODEL

In this section, we present the OTFS modulator and exclude the equations related to the receiver and channel, as this paper focuses on designing the OTFS transmit waveform.

A. OTFS modulator

Consider a two-dimensional OTFS frame $\mathbf{X}_{\text{DD}} \in \mathbb{C}^{M\times N}$ where each element $x_{DD}[k,l],, k \in \{0,1,...,M-1\}, l \in \{0,1,...,N-1\}$ represents modulated communication symbols, such as M-array QAM, in the DD domain. This frame is mapped to the TF domain using the Inverse Symplectic Finite Fourier Transform (ISFFT), a preprocessing step for OFDM modulation [12]. The TF representation, denoted as $\mathbf{X}_{\text{TF}} \in \mathbb{C}^{N\times M}$, is obtained by sampling the time and frequency axes at intervals ΔT and $\Delta f = 1/\Delta T$, respectively. Consequently, the frame duration is $T_f = N\Delta T$, and the total bandwidth is $B = M\Delta f = 1/T$. Applying ISFFT transforms the OTFS frame as,

$$x_{\text{TF}}[n,m] = \frac{1}{\sqrt{NM}} \sum_{k=0}^{M-1}\sum_{l=0}^{N-1} x_{\text{DD}}[k,l] e^{j2\pi\left(\frac{nl}{N}-\frac{mk}{M}\right)} \tag{1}$$

where $x_{\text{TF}}[n,m], n \in \{0,1,...,N-1\}, m \in \{0,1,...,M-1\}$ are the TF samples.This operation corresponds to applying the Discrete Fourier Transform (DFT) along one dimension (Doppler) and the Inverse Discrete Fourier Transform (IDFT) along the other (delay), yielding a matrix form,

$$\mathbf{X}_{\text{TF}} = (\mathbf{F}_M \mathbf{X}_{\text{DD}} \mathbf{F}_N^H)^T \tag{2}$$

where $\mathbf{F}_M \in \mathbb{C}^{M\times M}$ and $\mathbf{F}_N^H \in \mathbb{C}^{N\times N}$ are the unitary M-point DFT and the N-point IDFT matrices, respectively, i.e. $\mathbf{F}_M[l,m] = \frac{1}{\sqrt{M}} e^{-j2\pi l\frac{m}{M}}$. We further use this matrix format to solve the proposed optimization problem. To generate the continuous-time transmit signal, the Heisenberg transform with $g_{tx}(t)$ as the pulse-shaping function, is applied at each ΔT symbol duration, $n \in \{0,1,...,N-1\}$,

$$s_n(t) = \frac{1}{\sqrt{M}} \sum_{m=0}^{M-1} x_{\text{TF}}[n,m] e^{j2\pi m\Delta f t} g_{tx}(t),\ 0 \le t \le \Delta T \tag{3}$$

[1]**Notation**: $\mathbb{C}^N$ denotes the N-dimensional set of complex numbers. Bold uppercase $\mathbf{X}$ and lowercase $\mathbf{x}$ represent matrices and vectors, respectively. $\mathbf{X}^*$, $\mathbf{X}^T$, $\mathbf{X}^H$, $|\mathbf{X}|$, $\max(\mathbf{X})$, $\min(\mathbf{X})$, $\text{tr}(\mathbf{X})$, and $\text{vec}(\mathbf{X})$ represent the conjugate, transpose, Hermitian transpose, absolute value, maximum, minimum, trace, and vectorization of $\mathbf{X}$, respectively. $\text{diag}(\mathbf{x})$ is a diagonal matrices whose diagonal entries are equal to the elements of $\mathbf{x}$. Functions $\ln(.)$, $\text{rect}(.)$, and $\text{sinc}(.)$ denote logarithmic, rectangular, and sinusoidal functions. ∇_X is the gradient operation w.r.t. the variable X. $\Re$ and $\Im$ are the real and imaginary parts of a complex number, respectively.

Considering a rectangular pulse-shaping, the baseband transmit signal can be written as $s(t) = \frac{1}{\sqrt{N}}\sum_{n=0}^{N-1} s_n(t-n\Delta T)$ [15]. Thus, we have,

$$s(t) = \frac{1}{\sqrt{NM}} \sum_{n=0}^{N-1}\sum_{m=0}^{M-1} x_{\text{TF}}[n,m] e^{j2\pi m\Delta f(t-n\Delta T)} rect(t-n\Delta T). \tag{4}$$

B. Ambiguity Function of OTFS Waveform

From a radar perspective, the AF is a crucial performance metric to consider when designing waveforms. We derive the AF for the OTFS waveform, which can be computed for different delay shifts τ and Doppler frequencies f_d. For a general transmit signal $s(t)$, it is given by,

$$\chi(\tau, f_d) = \int_{-\infty}^{\infty} s(t) s^*(t-\tau) e^{j2\pi f_d t}\, dt, \tag{5}$$

Substituting $s(t)$ of Eq. (4) into Eq. (5), the AF of OTFS can be obtained by Eq. (7), shown at the top of the next page, where T_{diff} and T_{avg} can be calculated as follows [20]–[22],

$$\begin{aligned}
T_{\text{diff}}[n,n',T] &= \begin{cases} T_{max}-T_{min}, & \frac{\tau}{T}-1 < n-n' < \frac{\tau}{T}+1 \\ 0, & \text{other,} \end{cases} \\
T_{\text{avg}}[n,n',T] &= \begin{cases} \frac{T_{min}+T_{max}}{2}, & \frac{\tau}{T}-1 < n-n' < \frac{\tau}{T}+1 \\ 0, & \text{other,} \end{cases} \\
T_{\text{min}}[n,n',T] &= \max\{nT, n'T+\tau\}, \\
T_{\text{max}}[n,n',T] &= \min\{(n+1)T, (n'+1)T+\tau\}.
\end{aligned} \tag{6}$$

The ideal AF should have a single peak at the origin of the range-velocity plane, with zero values elsewhere. However, achieving a perfect AF is impossible. Radar waveform design aims to approximate this ideal by concentrating energy in the main lobe while minimizing sidelobes.The PSL of the AF plays a crucial role in determining radar resolution. In the next section, we formulate an optimization problem to enhance the OTFS waveform and improve its sensing capability through PSL minimization of the OTFS AF.

III. OTFS WAVEFORM OPTIMIZATION

A. Problem Formulation

To mitigate high sidelobes, we propose a phase-perturbed OTFS-based waveform design. This approach constructs a phase matrix, i.e., $\mathbf{\Theta}$, modifying the OTFS frame as:

$$\mathbf{X}'_{DD} = \mathbf{X}_{DD} \odot e^{j\mathbf{\Theta}}, \tag{8}$$

in order to improve sidelobe levels. Specifically, $\mathbf{\Theta}$ is designed to optimize the AF of the modified OTFS frame, $\chi'(\tau_i, d_j)$. By applying phase perturbations to each communication symbol in the DD domain, AF sidelobes are effectively suppressed, enhancing radar performance [21].

In (9), the optimization objective controls sidelobe levels across different range and Doppler lags, with weighting factors w_{ij} adjusting the emphasis on suppression in specific AF regions. To reduce computational complexity, the PSL can be optimized primarily near the mainlobe by setting $w_{ij} = 1$ if $(\tau_i, f_{dj}) \in \mathcal{A}$, and $w_{ij} = 0$ otherwise, where $\mathcal{A}$ defines the DD regions of interest.

$$\chi(\tau, f_d) = \sum_{m=0}^{M-1}\sum_{m'=0}^{M-1}\sum_{n=0}^{N-1}\sum_{n'=0}^{N-1} x_{\text{TF}}[n,m]x_{\text{TF}}^*[n',m']e^{j2\pi m'\Delta f\tau}\int_{T_{min}}^{T_{max}} e^{j2\pi((m-m')\Delta f+f_d)t}dt$$
$$= \sum_{m=0}^{M-1}\sum_{m'=0}^{M-1}\sum_{n=0}^{N-1}\sum_{n'=0}^{N-1} x_{\text{TF}}[n,m]x_{\text{TF}}^*[n',m']\underbrace{e^{j2\pi m'\Delta f\tau}T_{\text{diff}}[n,n']\text{sinc}\left(\pi((m-m')\Delta f+f_d)T_{\text{diff}}[n,n']\right)e^{j2\pi((m-m')\Delta f+f_d)T_{\text{avg}}[n,n']}}_{\tilde{\mathbf{A}}_{\tau,f_d}[n,m,n',m']} \quad (7)$$

$$\begin{cases} \min\limits_{\boldsymbol{\Theta}} \quad f(\boldsymbol{\Theta}) = \max\limits_{\substack{(\tau_i,f_{d_j})\in\mathcal{A}\\(\tau_i,f_{d_j})\neq(0,0)}} \left\{w_{ij}\left|\chi'(\tau_i,f_{d_j})\right|\right\} \\ s.t. \qquad |\boldsymbol{\Theta}[k,l]| \leqslant \theta_{max}, \begin{matrix}\forall k\in\{0,1,...,M-1\},\\ l\in\{0,1,...,N-1\}.\end{matrix}\end{cases} \quad (9)$$

Remark 1: If the phase perturbation applied to each DD symbol remains below the upper bound $\theta_{\max}$, the Signal to Noise Ratio (SNR) of the communication decreases by a factor of $\sin^2\left(\frac{\pi}{M}-\theta_{\max}\right)/\sin^2\left(\frac{\pi}{M}\right)$, where M represents the number of discrete phase levels in the modulation scheme, such as the number of symbols in an M-ary QAM scheme [21], [23]. Thus, $\theta_{\max}$ controls the trade-off between radar and communication functionalities. A small $\theta_{\max}$ significantly enhances radar sensing while causing only a negligible degradation in communication performance.

Remark 2: The matrix $\boldsymbol{\Theta}$ is not available at the communication receiver and is treated as phase noise. Thus, no modifications to existing communication processing schemes are required, allowing seamless integration with current systems.

Problem (9) is a min-max, nonlinear, non-convex and NP-hard optimization problem. We apply the epigraph reformulation and propose an Alternative Optimization (AO)-based algorithm. By decomposing the problem into two subproblems, we iteratively update the variables until convergence.

B. Solution to the optimization problem

To solve the problem (9), following a similar approach to that we proposed in [24], we introduce an auxiliary variable t, which constrains the objective function and transforms the min-max problem into a standard minimization problem. Therefore, by setting $w_{ij}=1$ for all $(\tau_i, f_{dj}) \in \mathcal{A}$, (9) can be reformulated as,

$$\begin{cases} \min\limits_{\boldsymbol{\Theta}} \quad t \\ s.t. \quad \begin{matrix}\left|\chi'(\tau_i,f_{d_j})\right| \leq t,\ \forall(\tau_i,f_{d_j})\in\mathcal{A},\ (\tau_i,f_{d_j})\neq(0,0)\\ |\boldsymbol{\Theta}[k,l]| \leqslant \theta_{max}, \begin{matrix}\forall k\in\{0,1,...,M-1\},\\ l\in\{0,1,...,N-1\}.\end{matrix}\end{matrix}\end{cases} \quad (10)$$

To handle the nonlinear and nonconvex constraint $\left|\chi'(\tau_i,f_{d_j})\right| \leq t$, we define a 4D array $\tilde{\mathbf{A}}_{\tau,f_d}[n,m,n',m'] \in \mathbb{C}^{N\times M\times N\times M}$, $n,n' \in \{0,1,...,N-1\}$, $m,m' \in \{0,1,...,M-1\}$ in Eq. (7) and reshape it into a 2D matrix $\mathbf{A}_{NM\times NM},\ \forall(\tau,f_d)$, that is, $A[\tilde{n},\tilde{m}] = \tilde{\mathbf{A}}[n,m,n',m']$ where $\tilde{n}=(n-1)M+m$, $\tilde{n}=(n'-1)M+m'$. This enables us to write the AF in (7) in a compact matrix form as,

$$\chi(\tau_i,f_{d_j}) = \text{vec}(\mathbf{X}_{\text{TF}})^H\mathbf{A}(\tau_i,f_{d_j})\text{vec}(\mathbf{X}_{\text{TF}}). \quad (11)$$

To express Eq. (11) in terms of the DD domain $\mathbf{X}_{\text{DD}}$, we use the vectorized form of the ISFFT (Eq. (2)) and apply the vec-Kronecker identity. Thus, we can write $\text{vec}(\mathbf{X}_{\text{TF}}) = (\mathbf{F}_M \otimes \mathbf{F}_N^*)\,\text{vec}(\mathbf{X}_{\text{DD}})$, and reformulate OTFS AF in DD domain as,

$$\chi(\tau_i,f_{d_j}) = \text{vec}(\mathbf{X}_{\text{DD}})^H\mathbf{H}(\tau_i,f_{d_j})\text{vec}(\mathbf{X}_{\text{DD}}), \quad (12)$$

where for each range-Doppler lag, $\mathbf{H}\in\mathbb{C}^{NM\times NM}$ is obtained by,

$$\mathbf{H}(\tau_i,f_{d_j}) = \left(\mathbf{F}_M^H\otimes\mathbf{F}_N^T\right)\mathbf{A}(\tau_i,f_{d_j})\ \left(\mathbf{F}_M\otimes\mathbf{F}_N^*\right)\forall(\tau_i,f_{d_j}) \quad (13)$$

To obtain the phase-perturbed OTFS AF $\chi'(\tau_i,f_{d_j})$, we use Eq. (8). Thus, we have,

$$\chi'(\tau_i,f_{d_j}) = \text{vec}(\mathbf{X}_{\text{DD}}\odot e^{j\Theta})^H\mathbf{H}(\tau_i,f_{d_j})\text{vec}(\mathbf{X}_{\text{DD}}\odot e^{j\Theta}). \quad (14)$$

Since $\mathbf{H}$ is not positive semi-definite (PSD), and due to the presence of the absolute value operation in the constraint $|\chi'(\tau_i,f_{d_j})| \leq t$, it is non-convex. By using the auxiliary variable $\mathbf{V}_{MN\times MN} = \text{vec}(\mathbf{X}_{\text{DD}}\odot e^{j\Theta})\,\text{vec}(\mathbf{X}_{\text{DD}}\odot e^{j\Theta})^H$, we have $\left|\chi'(\tau_i,f_{d_j})\right| = \left|\text{tr}(\mathbf{HV})\right| = \left|\sum_{i=1}^{MN}(\mathbf{HV})_{ii}\right|$. According to triangle inequality, $\left|\sum_{i=1}^{MN}(\mathbf{HV})_{ii}\right| \leq \sum_{i=1}^{MN}\left|(\mathbf{HV})_{ii}\right|$. Thus, we have $\left|\chi'(\tau_i,f_{d_j})\right| \leq \sum_{i=1}^{MN}\left|(\mathbf{HV})_{ii}\right|$. Minimizing the AF upper bound ($\sum_{i=1}^{MN}\left|(\mathbf{HV})_{ii}\right|$) ensures minimization of the AF itself. Thus, we can recast the optimization problem as,

$$\begin{cases} \min\limits_{\boldsymbol{\Theta},\mathbf{V},t} \quad t \\ s.t. \quad \begin{matrix}\sum\limits_{i=1}^{MN}\left|(\mathbf{H}(\tau_i,f_{d_j})\mathbf{V})_{ii}\right| \leq t,\ \begin{matrix}\forall(\tau_i,f_{d_j})\in\mathcal{A},\\(\tau_i,f_{d_j})\neq(0,0),\end{matrix}\\ |\boldsymbol{\Theta}[k,l]| \leqslant \theta_{max}, \begin{matrix}\forall k\in\{0,1,...,M-1\},\\ l\in\{0,1,...,N-1\}\end{matrix}\\ \mathbf{V} = \text{vec}(\mathbf{X}_{\text{DD}}\odot e^{j\Theta})\,\text{vec}(\mathbf{X}_{\text{DD}}\odot e^{j\Theta})^H.\end{matrix}\end{cases} \quad (15)$$

The problem remains nonconvex due to the equality constraint in $\mathbf{V}$ and its nonlinear relation with $\boldsymbol{\Theta}$. To address this, we first define the auxiliary variable $\mathbf{u} = \text{vec}(\mathbf{X}_{\text{DD}}\odot e^{j\Theta})$. Thus, $\mathbf{V} = \mathbf{u}\mathbf{u}^H$. We relax the problem w.r.t. the variable $\mathbf{V}$ and change the problem into a bi-objective optimization problem as follows, where η is a regularization parameter,

$$\begin{cases} \min\limits_{\boldsymbol{\Theta},\mathbf{V},t} \quad t+\eta||\mathbf{V}-\mathbf{u}\mathbf{u}^H||_F \\ s.t. \quad \begin{matrix}\sum\limits_{i=1}^{MN}\left|(\mathbf{H}(\tau_i,f_{d_j})\mathbf{V})_{ii}\right| \leq t,\ \begin{matrix}\forall(\tau_i,f_{d_j})\in\mathcal{A},\\(\tau_i,f_{d_j})\neq(0,0),\end{matrix}\\ |\boldsymbol{\Theta}[k,l]| \leqslant \theta_{max}, \begin{matrix}\forall k\in\{0,1,...,M-1\},\\ l\in\{0,1,...,N-1\}\end{matrix}\\ \mathbf{u} = \text{vec}(\mathbf{X}_{\text{DD}}\odot e^{j\Theta}).\end{matrix}\end{cases} \quad (16)$$

In this step, we decompose the problem into two subproblems and propose an AO-based approach that iteratively converges to the optimal solution. At each AO iteration, we first consider $\mathbf{\Theta}$ fixed, hence $\mathbf{u}$ is also fixed, and we solve the following subproblem (17), which is convex w.r.t. the variables $\mathbf{V}$ and t and can be solved with any convex optimization tool.

$$\begin{cases} \min\limits_{\mathbf{V},t} \quad g = t + \eta||\mathbf{V} - \mathbf{u}\mathbf{u}^H||_F \\ \\ s.t. \quad \sum\limits_{i=1}^{MN} \left|(\mathbf{H}(\tau_i, f_{d_j})\mathbf{V})_{ii}\right| \leq t, \ \begin{matrix}\forall(\tau_i, f_{d_j}) \in \mathcal{A}, \\ (\tau_i, f_{d_j}) \neq (0,0),\end{matrix} \end{cases} \tag{17}$$

Then, t and $\mathbf{V}$ are updated, and by fixing them, we solve the following subproblem (18) w.r.t. the variable $\mathbf{\Theta}$. Since $\mathbf{u}$ is a dependent and non-linear variable in this problem, we use Projected Gradient Descent (PGD) to solve it which is an extension of Gradient Descent (GD) incorporating a projection step to ensure that $\mathbf{\Theta}$ remains within the feasible set $|\mathbf{\Theta}[k,l]| \leqslant \theta_{max}$.

$$\begin{cases} \min\limits_{\mathbf{\Theta}} \quad ||\mathbf{V} - \mathbf{u}\mathbf{u}^H||_F \\ \\ s.t. \quad |\mathbf{\Theta}[k,l]| \leqslant \theta_{max}, \ \begin{matrix}\forall k \in \{0,1,...,M-1\}, \\ l \in \{0,1,...,N-1\}\end{matrix} \\ \quad\quad \mathbf{u} = \text{vec}(\mathbf{X}_{\text{DD}} \odot e^{j\mathbf{\Theta}}). \end{cases} \tag{18}$$

To compute the gradient $\nabla_{\mathbf{\Theta}} f(\mathbf{\Theta})$, $f(\mathbf{\Theta}) = ||\mathbf{V} - \mathbf{u}\mathbf{u}^H||_F$, we use the chain rule,

$$\nabla_{\mathbf{\Theta}} f(\mathbf{\Theta}) = \frac{\partial f}{\partial \mathbf{u}} \frac{\partial \mathbf{u}}{\partial \text{vec}(\mathbf{\Theta})} + \frac{\partial f}{\partial \mathbf{u}^*} \frac{\partial \mathbf{u}^*}{\partial \text{vec}(\mathbf{\Theta})}.$$

Since $f(\Theta) = \text{tr}((\mathbf{V} - \mathbf{u}\mathbf{u}^H)(\mathbf{V} - \mathbf{u}\mathbf{u}^H)^H)$, the derivative of f w.r.t. $\mathbf{u}$ is calculated as $\frac{\partial f}{\partial u} = -2\Re\{\mathbf{V}\}\mathbf{u} + 4\mathbf{u}\mathbf{u}^H\mathbf{u}$. Therefore, the gradient is calculated by [25],

$$\nabla_{\mathbf{\Theta}} f(\mathbf{\Theta}) = -4\Im\left(\text{diag}(\mathbf{u})(2\|\mathbf{u}\|^2\mathbf{I}_{MN} - \Re(\mathbf{V}))\mathbf{u}\right), \tag{19}$$

In the p^{th} iteration of the GD approach, $\mathbf{\Theta}$ is updated by,

$$\text{vec}(\mathbf{\Theta}^{(p)}) = \mathcal{P}_{\mathcal{C}}(\text{vec}(\mathbf{\Theta}^{(p-1)}) - \alpha\nabla_{\Theta} f(\mathbf{\Theta}^{(p-1)})) \tag{20}$$

where α is the step size and $\mathcal{P}_{\mathcal{C}}(.)$ is the projection operator such that $\mathcal{P}_{\mathcal{C}}(\mathbf{\Theta}) = \min(\max(\mathbf{\Theta}, \theta_{\min}), \theta_{\max})$. We iteratively update $\mathbf{\Theta}$ until convergence. Subsequently, the updated $\mathbf{\Theta}$ and $\mathbf{u}$ are fed into the algorithm as inputs for the next AO iteration to solve the first subproblem (17) again. The entire procedure is then iteratively repeated until the convergence criterion is satisfied. **Algorithm 1** summarizes the proposed approach.

IV. Numerical Results

In this section, we present numerical results to evaluate the performance of the proposed algorithm. Fig. 1 illustrates the normalized objective functions at each iteration of **Algorithm 1** under different settings. The decreasing cost functions confirm the convergence of the proposed approach.

We assume transmit pulses with a total bandwidth of $B = 200$ MHz and a pulse duration of $T_f = 320$ ns. The OTFS frame is constructed using a frame size of $M = N = 8$, where Quadrature Phase Shift Keying (QPSK) symbols are

Algorithm 1 Proposed AO-based algorithm for OTFS Waveform Optimization

Inputs: $\mathbf{X}_{\text{DD}}$, regularization parameter η, step size α, θ_{min}, θ_{max}, threshold ϵ and initialize $\mathbf{\Theta}^{(0)}$.
Outputs: Optimized phase matrix $\mathbf{\Theta}^{\star}$ and $\mathbf{X}'^{\star}_{DD}$.
Initialize $\mathbf{u}^{(0)} = \text{vec}(\mathbf{X}_{\text{DD}} \odot e^{j\mathbf{\Theta}^{(0)}})$.
for $q = 0, 1, 2, \ldots$ **do** (AO iteration)
    Solve the convex subproblem (17),
    Update $\mathbf{V}^{(q)}$ and $t^{(q)}$,
    for $p = 0, 1, 2, \ldots$ **do** (solving subproblem (18))
        Compute the gradient (19)
        update $\mathbf{\Theta}^{(p)}$ using the PGD update rule (20)
        Break if $||\mathbf{\Theta}^{(p-1)} - \mathbf{\Theta}^{(p)}||_F < \epsilon$.
    end for
    Update $\mathbf{\Theta}^{(q)} = \mathbf{\Theta}^{(p)}$,
    Update $\mathbf{u}^{(q)} = \text{vec}(\mathbf{X}_{\text{DD}} \odot e^{j\mathbf{\Theta}^{(q)}})$.
    Break if $|g^{(q-1)} - g^{(q)}| < \epsilon$.
end for
Outputs: $\mathbf{\Theta}^{\star} = \mathbf{\Theta}^{(q)}$ and $\mathbf{X}'^{\star}_{DD} = \mathbf{X}_{DD} \odot e^{j\mathbf{\Theta}^{\star}}$.

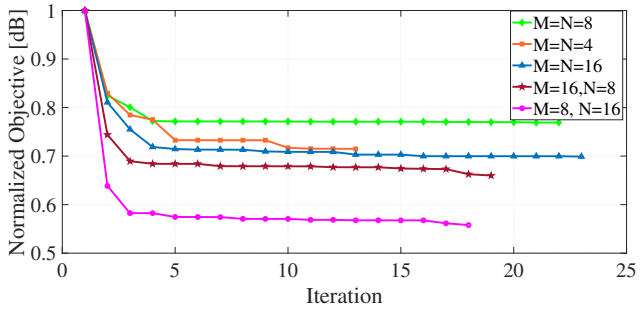

Fig. 1: Objective values of the proposed algorithm for different frame sizes.

embedded in each frame. Additionally, we set $\theta_{max} = 15°$. The region of interest $\mathcal{A}$ for sidelobe level reduction is defined by $w_{ij} = 1$, $\forall(\tau_i, f_{dj}) \in \mathcal{A} = [-0.2, 0.2]^2$ (normalized delay and Doppler frequencies w.r.t. the T_f and B, respectively). Fig. 2a and Fig. 2b show zero-Doppler and zero-delay cuts of the AF of initial and phase-perturbed OTFS signals, respectively. From these figures, it can be seen that, in the region $\mathcal{A}$ highlighted in the figures, the designed phase-perturbed OTFS exhibit lower sidelobe levels in both range and Doppler direction, leading to improved sensing performance. Since the algorithm focuses on sidelobe suppression only in $\mathcal{A}$, the sidelobe levels may be higher outside of this region. The 2D AF PSL values, PSL $= 10\log_{10}(\max_{(i,j)\neq(0,0)}(|\chi(\tau_i, f_{d_j})|^2))$, in the region $\mathcal{A}$, for the initial and designed waveforms are -16.57dB and -21.8dB respectively. Although the sidelobe level reduction is lower compared to our previous work in [20], the algorithm does not focus on a single dimension. Instead, in this paper, we achieve sidelobe suppression in two dimensions.

V. Conclusion

This paper proposes an optimization framework to design a phase-perturbed OTFS waveform aimed at improving radar

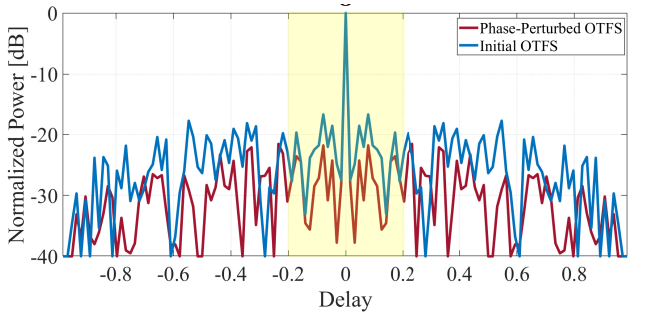

(a)

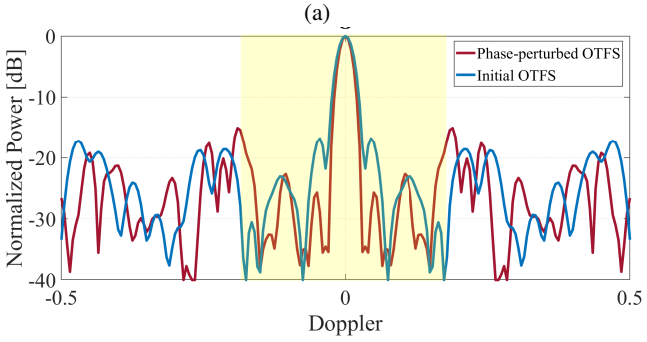

(b)

Fig. 2: (a) Zero-Doppler and (b) Zero-Delay sections of the OTFS waveform Ambiguity Functions.

sensing performance by reducing sidelobe levels in the DD domain. The approach minimizes the AF PSL in two dimensions while maintaining communication efficiency. The optimization problem is non-convex, and an AO-based algorithm is introduced to solve it iteratively across two subproblems: one convex and the other solved using the PGD approach. This ensures the feasibility of the solution while achieving PSL minimization. Numerical results show that the proposed algorithm effectively suppresses sidelobe levels in both range and Doppler dimensions, enhancing radar detection accuracy and reducing interference.

REFERENCES

[1] W. Yuan, Z. Wei, S. Li, J. Yuan, and D. W. K. Ng, "Integrated sensing and communication-assisted orthogonal time frequency space transmission for vehicular networks," *IEEE Journal of Selected Topics in Signal Processing*, vol. 15, no. 6, pp. 1515–1528, 2021.

[2] K. V. Mishra, M. R. Bhavani Shankar, V. Koivunen, B. Ottersten, and S. A. Vorobyov, "Toward millimeter-wave joint radar communications: A signal processing perspective," *IEEE Signal Processing Magazine*, vol. 36, no. 5, pp. 100–114, 2019.

[3] W. Zhai, X. Wang, M. S. Greco, and F. Gini, "Reinforcement learning based integrated sensing and communication for automotive MIMO radar," in *2023 IEEE Radar Conference (RadarConf23)*, 2023, pp. 1–6.

[4] R. Hadani, S. Rakib, A. F. Molisch, C. Ibars, A. Monk, M. Tsatsanis, J. Delfeld, A. Goldsmith, and R. Calderbank, "Orthogonal time frequency space (OTFS) modulation for millimeter-wave communications systems," in *2017 IEEE MTT-S International Microwave Symposium (IMS)*, 2017, pp. 681–683.

[5] R. Hadani, S. Rakib, M. Tsatsanis, A. Monk, A. J. Goldsmith, A. F. Molisch, and R. Calderbank, "Orthogonal time frequency space modulation," in *2017 IEEE Wireless Communications and Networking Conference (WCNC)*, 2017, pp. 1–6.

[6] J. K. Francis, R. Mary Augustine, and A. Chockalingam, "Diversity and papr enhancement in OTFS using indexing," in *2021 IEEE 93rd Vehicular Technology Conference (VTC2021-Spring)*, 2021, pp. 1–6.

[7] G. D. Surabhi and A. Chockalingam, "Low-complexity linear equalization for 2×2 mimo-otfs signals," in *2020 IEEE 21st International Workshop on Signal Processing Advances in Wireless Communications (SPAWC)*, 2020, pp. 1–5.

[8] J. Guetlein-Holzer, A. Kirschner, and J. Detlefsen, "Motion compensation for a TDM FMCW MIMO radar system," 01 2013, pp. 37–40.

[9] A. Gunturu, A. R. Godala, A. K. Sahoo, and A. K. R. Chavva, "Performance analysis of OTFS waveform for 5G NR mmwave communication system," in *2021 IEEE Wireless Communications and Networking Conference (WCNC)*, 2021, pp. 1–6.

[10] A. S. Bora, K. T. Phan, and Y. Hong, "Spatially correlated mimo-otfs for leo satellite communication systems," in *2022 IEEE International Conference on Communications Workshops (ICC Workshops)*, 2022, pp. 723–728.

[11] H. Wen, W. Yuan, and S. Li, "Downlink otfs non-orthogonal multiple access receiver design based on cross-domain detection," in *2022 IEEE International Conference on Communications Workshops (ICC Workshops)*, 2022, pp. 928–933.

[12] A. S. Bondre and C. D. Richmond, "Dual-use of OTFS architecture for pulse doppler radar processing," in *2022 IEEE Radar Conference (RadarConf22)*, 2022, pp. 1–6.

[13] M. F. Keskin, H. Wymeersch, and A. Alvarado, "Radar sensing with OTFS: Embracing ISI and ICI to surpass the ambiguity barrier," in *2021 IEEE International Conference on Communications Workshops (ICC Workshops)*, 2021, pp. 1–6.

[14] L. Gaudio, M. Kobayashi, G. Caire, and G. Colavolpe, "Joint radar target detection and parameter estimation with mimo otfs," in *2020 IEEE Radar Conference (RadarConf20)*, 2020, pp. 1–6.

[15] ——, "On the effectiveness of otfs for joint radar parameter estimation and communication," *IEEE Transactions on Wireless Communications*, vol. 19, no. 9, pp. 5951–5965, 2020.

[16] S. E. Zegrar, H. Haif, and H. Arslan, "Otfs-based isac for super-resolution range-velocity profile," *IEEE Transactions on Communications*, vol. 72, no. 7, pp. 3934–3946, 2024.

[17] S. Jiang and A. Alkhateeb, "Sensing aided otfs massive mimo systems: Compressive channel estimation," in *2023 IEEE International Conference on Communications Workshops (ICC Workshops)*, 2023, pp. 794–799.

[18] K. R. R. Ranasinghe, H. S. Rou, and G. T. F. de Abreu, "Fast and efficient sequential radar parameter estimation in mimo-otfs systems," in *ICASSP 2024 - 2024 IEEE International Conference on Acoustics, Speech and Signal Processing (ICASSP)*. IEEE, Apr. 2024, p. 8661–8665. [Online]. Available: http://dx.doi.org/10.1109/ICASSP48485.2024.10446001

[19] M. Jafri, S. Srivastava, and A. K. Jagannatham, "Sparse target parameter and channel estimation in mmwave mimo otfs-aided integrated sensing and communication systems," *IEEE Transactions on Communications*, pp. 1–1, 2024.

[20] N. Karimian-Sichani, M. Alaee-Kerahroodi, M. S. Greco, F. Gini, and B. S. M. R., "Otfs for automotive radars: Waveform optimization and ambiguity function analysis," in *Proceedings of the IEEE International Conference on Acoustics, Speech, and Signal Processing (ICASSP)*. Hyderabad, India: IEEE, April 2025.

[21] G. Song, J. Bai, and G. Wei, "An otfs-dfrc waveform design method based on phase perturbation," *IEEE Communications Letters*, vol. 27, no. 10, pp. 2578–2582, 2023.

[22] L. Qi, Y. Yao, B. Huang, and G. Wu, "A phase-coded OFDM signal for radar-communication integration," in *2019 IEEE International Symposium on Phased Array System and Technology (PAST)*, 2019, pp. 1–4.

[23] S. Zhou, X. Liang, Y. Yu, and H. Liu, "Joint radar-communications co-use waveform design using optimized phase perturbation," *IEEE Transactions on Aerospace and Electronic Systems*, vol. 55, no. 3, pp. 1227–1240, 2019.

[24] N. Karimian-Sichani, S. Sedighi, M. S. Greco, and F. Gini, "2d pilot signal design for otfs-isac systems," in *Proceedings of the International Radar Conference*. Pisa, Italy: IEEE, April 2025.

[25] K. Petersen and M. Pedersen, *The Matrix Cookbook*. Technical University of Denmark, 2006, version 20051003.